BULLETIN OF THE POLISH ACADEMY OF SCIENCES
TECHNICAL SCIENCES, Vol. 68, No. 6, 2020
DOI: 10.24425/bpasts.2020.135384

Design of nonlinear electromagnetic energy harvester equipped with mechanical amplifier and spring bumpers

M. OSTROWSKI[1], B. BŁACHOWSKI[1*], M. BOCHEŃSKI[2], D. PIERNIKARSKI[2], P. FILIPEK[3], and W. JANICKI[4]

[1] Institute of Fundamental Technological Research, Polish Academy of Sciences, ul. Pawińskiego 5b, 02-106 Warsaw, Poland
[2] Faculty of Mechanical Engineering, Lublin University of Technology, ul. Nadbystrzycka 36, 20-618 Lublin, Poland
[3] Faculty of Electrical Engineering and Computer Science, Lublin University of Technology, ul. Nadbystrzycka 38A, 20-618 Lublin, Poland
[4] Faculty of Earth Sciences and Spatial Management, Maria Curie-Sklodowska University, Al. Kraśnicka 2d, 20-718 Lublin, Poland

Abstract. The main drawback of vibration-based energy harvesting is its poor efficiency due to small amplitudes of vibration and low sensitivity at frequencies far from resonant frequency. The performance of electromagnetic energy harvester can be improved by using mechanical enhancements such as mechanical amplifiers or spring bumpers. The mechanical amplifiers increase range of movement and velocity, improving also significantly harvester efficiency for the same level of excitation. As a result of this amplitude of motion is much larger comparing to the size of the electromagnetic coil. This in turn imposes the need for modelling of electromagnetic circuit parameters as the function of the moving magnet displacement. Moreover, high velocities achieved by the moving magnet reveal nonlinear dynamics in the electromagnetic circuit of the energy harvester. Another source of nonlinearity is the collision effect between magnet and spring bumpers. It has been shown that this effect should be carefully considered during design process of the energy harvesting device. The present paper investigates the influence of the above-mentioned nonlinearities on power level generated by the energy harvester. A rigorous model of the electromagnetic circuit, derived with aid of the Hamilton's principle of the least action, has been proposed. It includes inductance of the electromagnetic coil as the function of the moving magnet position. Additionally, nonlinear behaviour of the overall electromagnetic device has been tested numerically for the case of energy harvester attached to the quarter car model moving on random road profiles. Such a source of excitation provides wide band of excitation frequencies, which occur in variety of real-life applications.

Key words: energy harvesting, velocity amplification, nonlinear electromagnetic circuit, spring bumper, quarter car model.

1. Introduction

Energy harvesting is a process of conversion of mechanical, thermal and other sources of energy into a usable form – usually related to electrical energy [1]. Development of energy harvesting is driven by modern energy-saving electronics and decreasing prices of modules used. Variety of DC/DC converters, e.g. highly efficient step-up or flyback converters allows us to easily adjust the voltage of the energy harvesting system to different powered devices [2, 3]. Many solutions for vibration-based energy harvesting devices are available. They can be classified based on their structure, topology or energy conversion mechanism utilising different type of motion and frequency range [4]. In this study vibration-based electromagnetic energy harvesters (EMEHs) are taken into consideration. The main motivation for this choice is high potential of EMEH in many applications due to inexpensive and easily accessible materials used. According to the Faraday's law, only wire coil and a moving magnet are required to cause electromechanical coupling effect [5]. Despite relatively simple structure and easily accessible materials mathematical modelling of the EMEHs is a quite complex task, because of inherent multi-physics associated with this problem [6]. Another advantage of EMEH devices is their high reliability. For that reason they can be successfully applied in very demanding engineering tasks of such as structural health monitoring, as it was shown in [7]. Another example is application of the energy harvester as self-powered magnetorheological dampers for vibration attenuation [8].

EMEHs exhibit relatively good performance, but the levels of generated power are still not sufficient for many potential applications where wireless power supply could be profitable. The simple way to improve the efficiency of the energy harvesting process is based on amplification of the range of motion, e.g. using pendulum-based mechanism [9]. It is also possible to use simple mechanisms called mechanical amplifiers, which transfer the low amplitude motion between two bodies into the high amplitude one [10].

Another way to increase the level of generated power is known as frequency-up conversion. Frequency bandwidth of energy harvester can be increased by means of additional preliminary vibrating system, which absorbs low-frequency vibration energy and transfers it into a high-frequency vibration of secondary system. Energy harvesters based on this mechanism

*e-mail: bblach@ippt.pan.pl

Manuscript submitted 2020-07-01, initially accepted for publication 2020-08-06, published in December 2020

are often non-resonant. Several examples of conversion mechanisms are shown in paper [11]. Another example of this kind of mechanism is free mass moving between less-massive magnets on springs. In this case collisions cause high-frequency vibrations inside the coils [12]. High amplification of velocity can also be achieved by elastic collisions of the moving magnet with other elements with larger masses [13]. In this way generated power has been increased 33 times compared to a single mass system. Furthermore, the structure was working in a significantly wider frequency bandwidth. A system based on the same principle, but different arrangement, is discussed in [14]. Also, the structure with a stroke of a magnet with end washers or elastic rubber bumpers, increases the level of the generated power and significantly expands the range of operational EMEH frequency [15, 16].

Another way to broaden the operational frequency bandwidth and increase harvester efficiency is a design of the so-called potential well, as shown in [17]. It has been observed that in nonlinear systems greater amplitudes do not guarantee greater power generated by EMEH. Zhang et al. in [18] have shown theoretically that a proper design of the potential well can guarantee so-called global resonance, i.e. that work done by excitation is always positive if some conditions related to the excitation are fulfilled. In engineering applications real time tuning can be viable.

Zhang et al. in [18] also indicate that the operational frequency bandwidth criterion can be misleading in considering the efficiency of energy harvesters, because in many cases power generated at resonance decreases with expansion of the frequency bandwidth. Thus, many devices work more efficiently out of the resonance at the expense of available efficiency under resonance. It is true, however, that the cited paper does not include considerations of the proportion between generated power and amplitude of vibration, e.g. of a moving magnet in the case of EMEH systems. Smaller efficiency at the resonance is the result of lower amplitudes, which determine smaller dimensions of the system. Considering this issue, one can show that expansion of the operational frequency bandwidth can still be profitable, which is one of the topics of the present paper.

The problem of extending the frequency bandwidth at the expense of the vibration at resonance can be avoided using self-tunable energy harvesters [19]. However, the structure of such devices is usually complex, making the design procedure more difficult. The system parameters supplied also have the influence on the generated power level. Due to the modern transducers, the input resistance of the system can be widely modified, so the value of the load resistance can also be a design parameter for the overall EMEH system [20].

In the present paper the influence of the mechanical amplifier and spring bumpers, imposing magnet stroke, on the EMEH work efficiency is discussed. Proportion between the level of mean generated power and the dimensions of the analysed EMEH device is also examined. For benchmark purposes dimensions and properties of the coil and moving magnet adopted in this paper are similar to those of EMEH device shown in [21]. In this paper electromechanical coupling has been determined numerically using the Biot-Savart law for similarity between the field of the magnet and the field induced by solenoid replacement, as shown in [22]. The mathematical model of the electrical circuit presented in [21] include only constant coil inductance, which does not depend on the position of the magnet (here as an iron core inside the coil). However, for large displacements and velocities of the magnet, a mathematical model of the electric circuit should be refined in order to describe its nonlinear dynamics. In this paper a mathematical model of the EMEH device has been derived by using Hamilton's principle of least action. Nonlinear behaviour is typical for the electromagnetic devices and mathematically well-described [23]. However, for the EMEH devices the nonlinear terms depend also on the mechanical part of the system. In the present study it is assumed that, coil inductance depends on the magnet position, and force, derived from the reluctance of the magnetic circuit, is also considered [24]. Based on the proposed mathematical model participation of the nonlinear terms in the dynamic response of EMEH has been studied. Additionally an examination of the influence of the design parameters on the EMEH efficiency has been also performed. A quarter car model moving on randomly generated road profiles has been employed as the source of vibration. The motivation is that vibration-based energy harvesters are often excited by random and nonperiodic forces.

Diagram presented in Fig. 1 shows all elements of the analysed dynamic system. The EMEH device and electrical load are described in detail in Section 2. The quarter car model moving on randomly generated road profiles and the mechanical amplifier are discussed in Section 3. Section 4 contains results of the parametric study and analysis of nonlinearities. The paper is concluded with enumeration of the most important aspects of EMEH in Section 5.

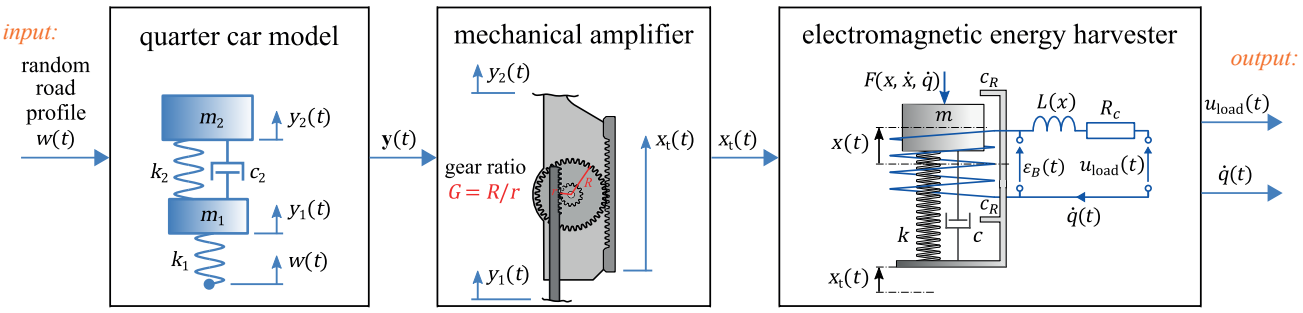

Fig. 1. The concept of vibration-based energy harvesting

2. Energy harvesting device

A schematic diagram of the studied model of EMEH is shown in Fig. 2. This model represents the EMEH device consisting of a tube (casing) made of non-magnetic material, a spring with stiffness k, a moving magnet with mass m, viscous damping with constant c and an electromagnetic coil attached to the tube. $x_t(t)$ and $x(t)$ are displacement of the tube and the relative displacement of the magnet with reference to the electromagnetic coil in the function of time t, respectively. The tube is equipped with two spring bumpers, which cause resilient collision. It is assumed that the length of these springs is very small and they have high stiffness. Hence, when the magnet reaches extreme relative displacement with respect to the coil $x_{\max}$, the influence of the spring bumpers on the moving magnet is modelled by the resilient collision described by the restitution coefficient $c_R = 0.9$. It follows that $x \in [-x_{\max}, x_{\max}]$.

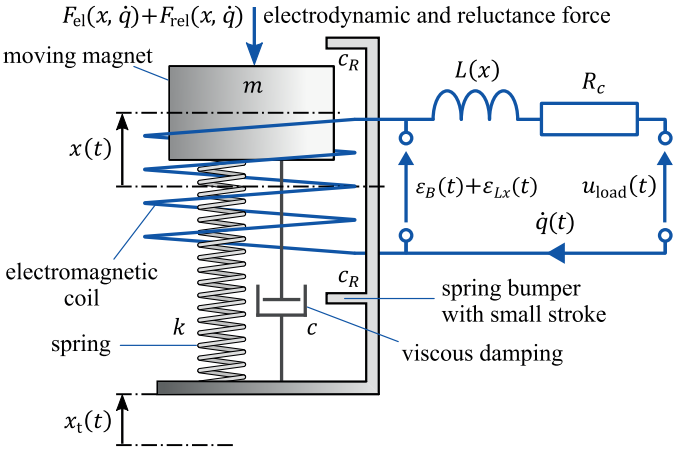

Fig. 2. Scheme of EMEH device

Electrical circuit shown in Fig. 2 consists of: inductance of the coil depending on the relative displacement of the magnet $L(x)$, resistance of the coil wire R_c, electromotive force $\varepsilon_B(t)$ caused by the magnetic field of the moving magnet, self-induced electromotive force ε_{Lx} caused by change of the inductance $L(x)$ and voltage across the load $u_{load}(t)$.

The electromotive force ε_B is generated in the coil turns by change of the magnetic flux linkage Φ induced by the moving magnet (Faraday's Law):

$$\varepsilon_B(t) = -\frac{\mathrm{d}}{\mathrm{d}t}\Phi(x(t)) = -\frac{\partial\Phi(x)}{\partial x}\dot{x}(t), \tag{1}$$

Gradient of the magnetic flux linkage shown in the equation above is called electromechanical coupling. The mechanical result of the electromechanical coupling is electrodynamic (Lorenz) force:

$$F_{el} = \frac{\partial\Phi(x)}{\partial x}\dot{q}, \tag{2}$$

where q is electrical charge – its time-derivative $\dot{q}$ is the electrical current in the electrical circuit. The reluctance force F_{rel} results from the change of the reluctance with magnet displacement. The exact dependence of reluctance force F_{rel} (mechanical part of the system) and voltage ε_{Lx} (electrical part) on the inductance in relation to x is derived in the next subsection.

The magnet and coil properties used in the numerical study in the paper are similar to the EMEH researched in [21]. These data are used in the present paper as a benchmark for generated power in the case where enhancements are not implemented, and were listed in Table 1.

Table 1
Magnet properties

description	symbol	value
magnet material	–	NdFeB (N38)
magnet height	h_m [mm]	35
magnet diameter	d_m [mm]	20
magnet mass	m [g]	90
magnet direction of magnetisation	–	Axis (–)
coil wire resistance	R_c [Ω]	1 200
coil inductance (without magnet inside)	L_{air} [H]	1.463
number of coil turns	N [–]	12 740

2.1. Dynamics of electromagnetic energy harvester. To properly understand dynamic interaction between mechanical and electrical part of the proposed energy harvester equations of motion of the overall system have to be assembled. The equations of motion were derived by employing Hamilton's principle of the least action. The action $\mathscr{I}$ is expressed by the equation below.

$$\mathscr{I} = \int_{t_1}^{t_2} \mathscr{L}\,\mathrm{d}t, \qquad t_1 < t_2, \tag{3}$$

where $\mathscr{L}$ is the Lagrangian:

$$\mathscr{L} = T^* + M^* - V - E \tag{4}$$

written in displacement and electric charge formulation [25]. Here T^* is kinetic coenergy, M^* is magnetic coenergy, V is mechanical potential energy and E is electrical potential energy. These quantities are described by the following formulas:

$$T^* = \frac{1}{2}m(\dot{x}+\dot{x}_t)^2, \tag{5}$$

$$M^* = \frac{1}{2}L(x)\dot{q}^2 + \Phi(x)\dot{q}, \tag{6}$$

$$V = \frac{1}{2}kx^2, \tag{7}$$

$$E \equiv 0. \tag{8}$$

The second term (6) relates to the mechanical work of the force F_{el} (see: Eq. (2)) done on electrical part of the system. It is also

a metric of energy exchange between mechanical and electrical part of the EMEH device through the magnetic field of the moving magnet.

The system has two degrees of freedom: relative displacement x and electric charge q. Conservative and dissipative forces should be taken into account. Hence, the Euler-Lagrange equations have the following form:

$$\begin{cases} \dfrac{\mathrm{d}}{\mathrm{d}t}\dfrac{\partial \mathscr{L}}{\partial \dot{x}} + \dfrac{\partial \mathscr{D}}{\partial \dot{x}} - \dfrac{\partial \mathscr{L}}{\partial x} = F, \\ \dfrac{\mathrm{d}}{\mathrm{d}t}\dfrac{\partial \mathscr{L}}{\partial \dot{q}} + \dfrac{\partial \mathscr{D}}{\partial \dot{q}} - \dfrac{\partial \mathscr{L}}{\partial q} = u, \end{cases} \tag{9}$$

where: F is external force, u is external voltage and

$$\mathscr{D} = \frac{1}{2}c\dot{x}^2 + \frac{1}{2}R_{\mathrm{c}}\dot{q}^2 \tag{10}$$

is dissipation function expressed in terms of power of the energy losses in the system. Only kinematic excitation acts on the magnet that is taken into account in equation (5), so $F \equiv 0$. For the system shown in Fig. 2 $u = u_{\mathrm{load}}$. Substituting equations (5)–(7) and (10) into (9) we receive equations of motion (11).

$$\begin{bmatrix} m & 0 \\ 0 & L(x) \end{bmatrix} \begin{bmatrix} \ddot{x} \\ \ddot{q} \end{bmatrix} + \begin{bmatrix} c & -\left(\dfrac{\partial \Phi}{\partial x} + \dfrac{1}{2}\dfrac{\partial L}{\partial x}\dot{q}\right) \\ \dfrac{\partial L}{\partial x}\dot{q} + \dfrac{\partial \Phi}{\partial x} & R_{\mathrm{c}} \end{bmatrix} \begin{bmatrix} \dot{x} \\ \dot{q} \end{bmatrix} + \begin{bmatrix} k & 0 \\ 0 & 0 \end{bmatrix} \begin{bmatrix} x \\ q \end{bmatrix} = \begin{bmatrix} -m\ddot{x}_{\mathrm{t}} \\ u_{\mathrm{load}} \end{bmatrix}. \tag{11}$$

The above equations contain nonlinearities associated with the dependence of the inductance and electromechanical coupling on relative displacement of the moving magnet x. It is worth noticing that off-diagonal elements of the matrix next to first-order derivatives of the response vector are responsible for coupling between mechanical and electrical part of the system. In Eq. (11) $\dfrac{1}{2}\dfrac{\partial L}{\partial x}\dot{q}^2 = F_{\mathrm{rel}}(x,\dot{q})$ and $\dfrac{\partial L}{\partial x}\dot{x}\dot{q} = \varepsilon_{Lx}(x,\dot{x},\dot{q})$.

Power P generated as a result of the load is expressed by the equation below.

$$P = -u_{\mathrm{load}}\dot{q}\,. \tag{12}$$

If the load is to be expressed as a resistance, the voltage across the load is expressed as follows:

$$u_{\mathrm{load}} = -R_{\mathrm{load}}\dot{q}\,. \tag{13}$$

Functions $L(x)$ and $\dfrac{\partial \Phi(x)}{\partial x}$ are calculated numerically in the next subsections.

2.2. Electromechanical coupling as the function of relative magnet displacement. The derivative of the magnetic flux linkage over magnet displacement fulfils the equation below.

$$\frac{\partial \Phi(x)}{\partial x} = \int_{l_{\mathrm{c}}} B_r(l)\,\mathrm{d}l \tag{14}$$

Here l_{c} is the length of the curve along the wire turns of the coil and B_r is the radial component (normal to the coil wire) of the magnetic field vector $\mathbf{B}$. In further calculations it was assumed that the field of the magnetic induction $\mathbf{B}$ of the magnet can be approximated by a field of a solenoid with the same dimensions [22]. It is also accepted that the magnet is divided into N_{m} solenoid loops, each with diameter d_{m}. The current in each such loop has a value calculated as follows:

$$I_m = \frac{B_r h_{\mathrm{m}}}{\mu_0 N_{\mathrm{m}}}, \tag{15}$$

where B_r is the residual magnetic field strength and μ_0 is permeability of the vacuum. Having I_{m} magnetic induction $\mathbf{B}$ at the point on the curve along the coil wire has been calculated using the Biot-Savarat law:

$$\mathbf{B} = \frac{\mu_0 I_{\mathrm{m}}}{4\pi}\int_{l_{\mathrm{m}}} \frac{\mathrm{d}\mathbf{l}\times\mathbf{r}}{r^3}, \tag{16}$$

where $\mathrm{d}\mathbf{l}$ is the vector differential length along curve l_{m} of the solenoid, $\mathbf{r}$ is the vector from the point on the solenoid to the point on the curve along the coil wire, r is the length of vector $\mathbf{r}$. Function $\dfrac{\partial \Phi(x)}{\partial x}$ has been calculated numerically for values $B_r = 1$ T and $N_{\mathrm{m}} = 20$ using MATLAB software. The assumed dimensions of the coil are listed in Table 2. It is assumed that the turns of coils are evenly distributed in the coil's cross section. The results are shown in Fig. 3, where the red dots denote the numerical result and the blue line denotes the fitted curve $\alpha(x)$. The fitting curve was assumed during these calculations that the range of the magnet motion is $l_x = 200$ mm (shown in Fig. 3). The function sought in interval l_x can be assumed to be one period with the length of l_x of a periodic function. Then curve $\alpha(x)$ can be expressed as a series of harmonic functions

Table 2
Dimensions of the coil assumed in calculations

description	symbol	value
axial length of the coil	h_c [mm]	55
outer diameter	D_c [mm]	28
inner diameter	d_c [mm]	23

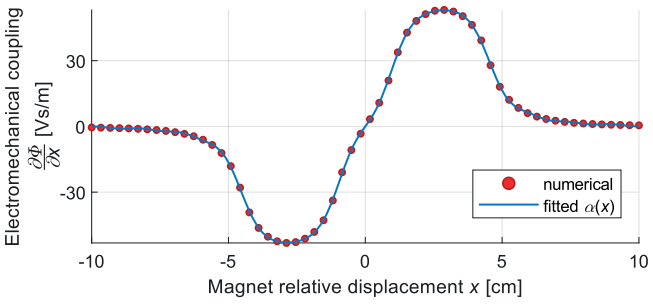

Fig. 3. Electromechanical coupling as a function of magnet displacement x

like in the Fourier series approximation. It is a convenient approach because of the orthogonality of the harmonic functions in period l_x. Function $\alpha(x)$ is described by Eq. (17).

$$\alpha(x) = \sum_{n=1}^{N_h} A_n \sin\left(\frac{2\pi n}{l_x} x\right). \tag{17}$$

Here coefficients A_n minimise the least square error between the numerically calculated coupling coefficient (red dots) and the fitted curve. It has been calculated that the number of harmonics $N_h = 13$ is sufficient to fit function $\alpha(x)$. The values of the coefficients A_n for $n = 1, 2 \ldots 13$ are listed in Table 3.

Table 3
Coefficients of Fourier series for electromechanical coupling

n	A_n [Vm/s]	n	A_n [Vm/s]	n	A_n [Vm/s]
1	29.5578	6	0.5466	11	0.0453
2	26.4298	7	0.4715	12	−0.2148
3	8.4275	8	−1.3008	13	−0.4254
4	−2.5786	9	−1.5718	–	–
5	−2.1949	10	−0.6452	–	–

Function $\alpha(x)$ is used in equations of motion (11) during numerical integration, where the $\alpha(x)$ values for the x outside the range shown in Fig. 3 are assumed equal to zero. Found $\alpha(x)$ function is in good agreement with the experimental results shown in [21]. Electromechanical coupling is an odd function of x, so oscillation of the magnet generates oscillations of the current in the electrical circuit with doubled frequency.

2.3. Inductance as function of relative magnet displacement. To determine inductance $L(x)$ a semi-analytical method shown in [24] was used. In this method calculation of the inductance is based on the Poisson partial differential Eq. (18) describing magnetic vector potential on the longitudinal section of the coil-iron core system shown in Fig. 4.

$$\frac{\partial^2 A}{\partial R^2} + \frac{1}{R}\frac{\partial A}{\partial R} - \frac{A}{R^2} + \frac{\partial^2 A}{\partial z^2} = -\mu_0 J(R,z). \tag{18}$$

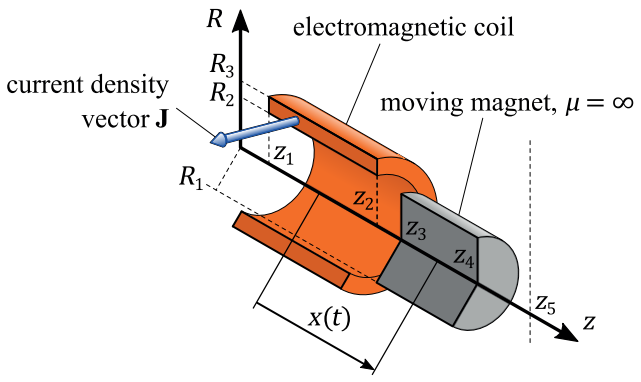

Fig. 4. Longitudinal section of the coil-core (magnet) considered in calculations of the inductance

Here A is a component of the magnetic potential vector field perpendicular to the longitudinal section, R denotes the radius from the axis of the coil, J is current density in the cross section of the coil for unit current in the coil expressed by formula

$$J(R,z) = \begin{cases} N/((R_3 - R_2)h_c) & \text{if } R_2 \le R \le R_3, \\ & z_1 \le z \le z_2, \\ 0 & \text{if } R,\ z \text{ elsewhere}, \end{cases} \tag{19}$$

where N is number of the coil turns (see: Table 1). 0 and z_5 are limits of the whole domain, at which $A = 0$. It does not determine dimensions of the EMEH device yet. Furthermore $0 \ll z_1$ and $z_4 \ll z_5$.

Solution of Eq. (18) can be given as a series of the Bessel functions and trigonometric functions as shown in detail in [24]. The results are shown in Fig. 5, where red dots denote a semi-analytical solution for different values of x. Semi-analytical solution has been obtained for 70 harmonics, $z_1 = 0.2475$ m, $z_2 = 0.3025$ m, $z_5 = 0.550$ m. z_3 and z_4 were varying according to the iron core (moving magnet) position. The blue line in Fig. 5 is the fitted curve described by Eq. (20), while $L_{air} = 1.463$ H is the inductance of the coil without core.

$$L(x) = L_{air} + \kappa_L e^{-\left(\frac{x}{\sigma_L}\right)^2}. \tag{20}$$

Parameters $\kappa_L = 3.6877$ H and $\sigma_L = 0.02665$ m have been determined by minimising the least square problem. Function in Eq. (20) is used in numerical integration of equations of motion (11). The advantages of function $L(x)$ are that it is easily differentiable, decreases with displacement of the magnet and achieves zero in infinity.

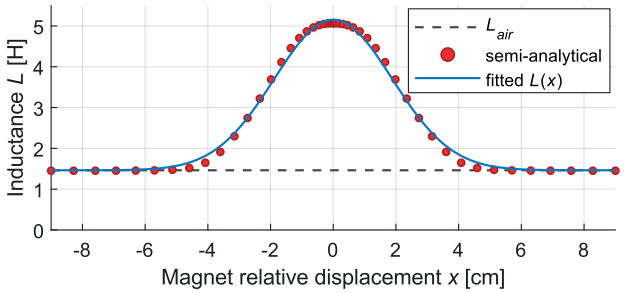

Fig. 5. Coil inductance as a function of magnet position

3. Mechanical model of a vehicle moving on uneven road

This section presents the quarter car model and the method of mounting a mechanical amplifier as well as the adopted method of road profile generation. These three parts constitute the environment of the EMEH device and allow for testing the device's efficiency.

3.1. Quarter car model. In the present study the quarter car model is used, because it is one of the simplest models which behaves similarly to the suspension of the whole vehicle. The

quarter car model is shown in Fig. 6 and consists of the lower, so-called unsprung mass m_1 simulating wheel and axle, the upper, so-called sprung mass m_2 simulating quarter part of the car body, stiffness k_1 representing tyre stiffness, suspension stiffness k_2 and suspension viscous damping factor c_2. $y_1(t)$ and $y_2(t)$ are displacements of the unsprung and sprung mass, respectively, $w(t)$ is the height of the road profile at time instant t, V is the velocity of the vehicle.

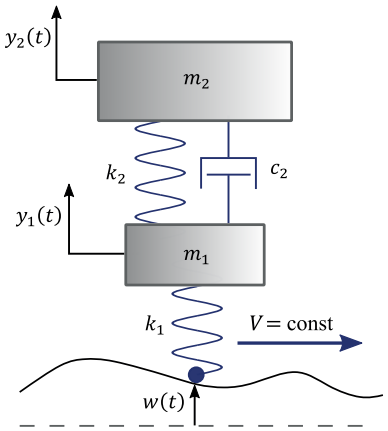

Fig. 6. Quarter car model

The quarter car model is described by the linear equation of motion (21), where tyre damping has been neglected because of its small value relative to the damping of the suspension.

$$\begin{bmatrix} m_1 & 0 \\ 0 & m_2 \end{bmatrix} \begin{bmatrix} \ddot{y}_1 \\ \ddot{y}_2 \end{bmatrix} + \begin{bmatrix} c_2 & -c_2 \\ -c_2 & c_2 \end{bmatrix} \begin{bmatrix} \dot{y}_1 \\ \dot{y}_2 \end{bmatrix} + \begin{bmatrix} k_1+k_2 & -k_2 \\ -k_2 & k_2 \end{bmatrix} \begin{bmatrix} y_1 \\ y_2 \end{bmatrix} = \begin{bmatrix} k_1 \\ 0 \end{bmatrix} w. \tag{21}$$

Values of all coefficients from Eq. (21) are selected so as to simulate the lorry, as described in [26]. They are listed together with modal parameters of the quarter car model in Table 4.

Table 4
Properties and modal parameters of the quarter car model

description	symbol	value
unsprung mass	m_1 [kg]	500
sprung mass	m_2 [kg]	4500
tire stiffness	k_1 [Nm/s]	$2 \cdot 10^6$
suspension stiffness	k_2 [Nm/s]	10^6
shock absorber damping coeff.	c_2 [Ns/m]	$2 \cdot 10^4$
undamped natural frequencies	ω_{u1} [rad/s]	12.10
	ω_{u2} [rad/s]	77.95
damped natural frequencies	ω_{d1} [rad/s]	12.14
	ω_{d2} [rad/s]	74.33
modal damping factors*	ξ_1 [%]	7.91
	ξ_2 [%]	27.28

* % of critical damping

3.2. Mechanical amplifier. If the EMEH can be placed between two relatively moving bodies, then a special kind of interface between the EMEH device and these moving bodies, called mechanical amplifier, can be used. Due to the relative motion between the bodies, the mechanical amplifier increases displacements of the EMEH device per unit of time, thus also increasing its velocities and accelerations. Examples of these simple mechanisms used in energy harvesters are discussed in [10]. Such a mechanism shown in Fig. 7 can be mounted between sprung and unsprung masses of the quarter car model shown in Fig. 6. Taking into account the equation of motion (21), the displacement of the energy harvester tube $x_t(t)$ from Eq. (11) is as follows:

$$x_t(t) = G[y_2(t) - y_1(t)] + y_1(t). \tag{22}$$

In these example a gain of motion G can be defined as the output-input amplitude ratio. The input amplitude is a direct result of the relative motion of the bodies.

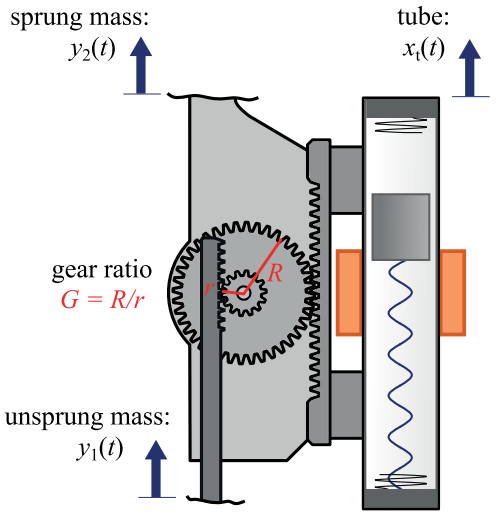

Fig. 7. Mechanical amplifier concept

3.3. Randomly generated road profiles. The International Organisation for Standardisation classified longitudinal road profiles according to their roughness (ISO 8608). Roughness is expressed by the power spectral density (PSD) values of the profile. It allows us to generate road profiles by re-derivation of a random series of sinusoidal functions. This method has been adopted from [27].

Most road profiles roughness can be expressed by PSD in the following way:

$$\Theta(\Omega) = \Theta(\Omega_0) \left(\frac{\Omega}{\Omega_0} \right)^{-2}, \tag{23}$$

where $\Omega = \dfrac{2\pi}{L_s}$ [rad/m] is angular spatial frequency, L_s is wavelength [m], and $\Omega_0 = 1$ rad/m. The values of the PSD $\Theta(\Omega_0)$ for different road classes are listed in Table 5.

Table 5
Degree of roughness for different road classes

road class	$\Theta(\Omega_0)$, $[10^{-6}\mathrm{m}^3]$		
	lower limit	geometric mean	upper limit
A	–	1	2
B	2	4	8
C	8	16	32
D	32	64	128
E	128	256	512

In this approach the re-derived random series of the sinusoidal functions has the form of Eq. (24).

$$w(t) = \sum_{i=1}^{N_W} W_i \sin\left(\Omega_i V t + \phi_i\right), \tag{24}$$

where $W_i = \sqrt{\Theta(\Omega_i)\dfrac{\Omega_N - \Omega_1}{\pi(N-1)}}$, $\Omega_i = i\Omega_1$, $\Omega_N = N_W\Omega_1$, $\phi_i \in [0, 2\pi)$ is a random variable with uniform probability distribution, N_W is the number of harmonics. The values of parameters are as follows: $\Omega_1 = 0.02\pi$ rad/m, $\Omega_N = 6\pi$ rad/m and thus $N_W = 300$. These values cover the bandwidths suggested by ISO 8608. The equation above is suitable only for $V = \text{const}$.

Examples of generated random road profiles in relation to the travelled distance $s = Vt$ for the road classes A and C are shown in Fig. 8. It can be seen that for the lower road class the roughness of the road is greater. The spatial harmonics content is the same according to Eq. (24), where amplitudes W_i are not random variables. Due to this property of the generated profile it is easy to determine the desired PSD value (see Eq. (23)).

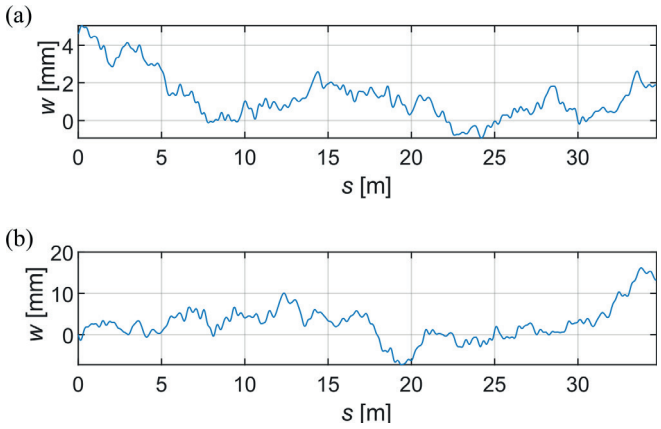

Fig. 8. Examples of randomly generated road profiles: (a) for the road class A, (b) for the road class C

4. Numerical study

This section presents a numerical study intended to calculate the level of generated power and show the behaviour of the EMEH device. In the following subsection an example of time histories of the state of the EMEH device for randomly generated road profile is shown. The third subsection addresses the characteristics of mean generated power in relation to different system parameters. Finally, the influence of nonlinearities of the modelled system is discussed.

4.1. Power generated by EMEH device. In this subsection behaviour of the EMEH equipped with the spring bumpers and the mechanical amplifier device is illustrated in exemplary time histories. In this case the load resistance $R_{\text{load}} = 2500\ \Omega$, gain $G = 20$ and the stiffness $k = 550$ N/m. This value of stiffness provides similar undamped natural frequency of the EMEH device $\omega_0 = \sqrt{k/m} = 78.17$ rad/s as the second natural frequency of the quarter car model ω_{u2}. It allows the EMEH device to get into resonance. In this subsection the road profile shown in Fig. 8(b) was used, whereas vehicle velocity was assumed to be equal $V = 50$ km/h to simulate behaviour of the EMEH while driving the vehicle on urban roads.

Figure 9 shows the displacement, corresponding accelerations of the EMEH tube (excitation), load voltage u_{load}, magnet displacement x and generated energy E for assumed maximum displacement $x_{\max} = 5$ cm and gain $G = 20$. Mean generated power has been calculated from the end value of the produced energy:

$$P_{\text{mean}} = \frac{1}{t_{\text{end}}} E(t_{\text{end}}), \tag{25}$$

where: $\dot{E}(t)$ is equal to the generated power in Eq. (12).

The frequency of the voltage is twice the vibration frequency of the moving magnet, because the electromechanical coupling is an odd function of magnet relative displacement x. Voltage occasionally achieves values greater than 200 V because of high number of coil turns. Mean power has a very rewarding value of $P_{\text{mean}} = 1.85$ W with relatively small dimensions of the EMEH device determined by $x_{\max}$ due to the use of the spring bumpers and the motion range amplifier. It can be seen that in time intervals when collision of the magnet with the spring bumpers does not occur, generated energy increments are significantly smaller. Also the level of generated voltage and electrical current are much smaller in these time intervals.

4.2. Influence of selected parameters on EMEH performance. This subsection discusses the characteristics describing dependences of the mean generated power and the values of the design parameters for selected road profiles and vehicle velocities.

The EMEH device is nonlinear and its characteristics have been determined by integration of equations of motion for each value of the parameters which influence the generated power. Furthermore, road profiles expressed by Eq. (24) are random and for each numerical test the time histories of the EMEH state (for example those shown in subsection 4.1) and the P_{mean} values will be different. The characteristics have been determined by calculating the average values of mean power from particular values of $P_{\text{mean}}^{(n)}$, each for n-th randomly generated road profile

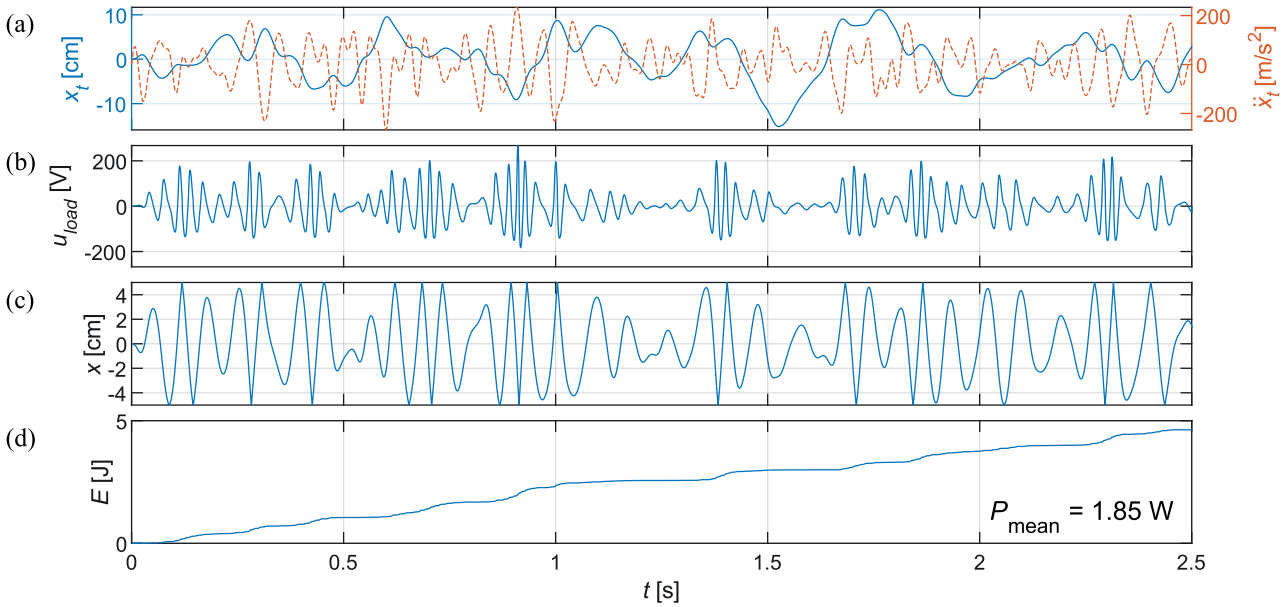

Fig. 9. Time histories of: (a) displacement and accelerations of the EMEH tube (red dashed line), (b) voltage produced by the EMEH device, (c) relative displacement of the moving magnet and (d) generated energy

$w_n(t)$ according to the formula below.

$$P_{\text{mean}} = \frac{1}{N_n} \sum_{n=1}^{N_n} P_{\text{mean}}^{(n)} . \tag{26}$$

For this research, the number of randomly generated road profiles $N_n = 50$. The results are shown in Fig. 10. For each iteration $t_{\text{end}} = 10$ s. The numerical study shows that longer time does not significantly affect the results.

For comparison, the generated power characteristics have been determined for two classes of the road: A and C and the corresponding values of vehicle velocity V: 110 km/h and 50 km/h, respectively, to simulate the system behaviour used on the urban roads as well as the motorways or expressways. For each of these two cases three types of characteristics have been determined:

- $x_{\max}$ vs R_{load}: parameters $x_{\max}$ and R_{load} vary, others are constant: $k = 550$ N/m, $G = 20$,
- k vs $x_{\max}$: parameters k and $x_{\max}$ vary, others are constant: $G = 20$, and $R_{\text{load}} = 2500\ \Omega$,
- $x_{\max}$ vs G: parameters $x_{\max}$ and G vary, others are constant: $k = 550$ N/m, $R_{\text{load}} = 2500\ \Omega$.

Generated power is greater for the case of smaller velocity V and worse road quality. Higher vehicle velocity V does not guarantee a significantly higher level of vibrations of the m_1 and m_2 masses of the model, but merely results in shifting the excitation bandwidth provided by the random road profiles into the higher frequencies. The exact dependence of the generated power P_{mean} on velocity V is difficult to analyse because the EMEH device is nonlinear system. Furthermore, in reality the road profile is unknown.

Areas where dependence of the P_{mean} value on the design parameters is more regular are visible in the characteristics shown in Fig. 10, cases (a), (c) and (e). These areas refer to situations where the stroke value $x_{\max}$ is greater than amplitude of the moving magnet motion. Thus no resilient collision with spring bumpers appears. Harvested power does not strongly depend on randomly generated road profile when the magnet does not reach the bumpers, because the road profiles have the same harmonics content. The random variable in the randomly generated road profile is only a phase shift (see Eq. (24)). In the cases when the magnet motion achieves sufficient amplitude to provide resilient collisions, the trajectory of the moving magnet changes significantly when a different phase shift of each particular harmonic appears for different random road profiles. This is the reason for the irregular shape of the plot of the characteristic when the magnet reaches $x_{\max}$ position, even for calculation of the mean power P_{mean} for 50 randomly generated road profiles. The maximum of the P_{mean} is shifted into higher values of the $x_{\max}$ parameter for worse road quality (outside the plots). The reason is that for higher vibration levels it is more expected that the moving magnet will have collision with the spring bumpers, even if they are set up with greater distance between them.

The red line exposed on the characteristics shown in Fig. 10 corresponds to the optimal ratio $P_{\text{mean}}/x_{\max}$. It is helpful in indicating the optimal dimensions of the EMEH device provided by the parameter $x_{\max}$. The characteristics show that use of the bumpers enhances the EMEH device in the sense of the proportion between P_{mean} and the size of the EMEH device. It can be seen that the optimal value of the $x_{\max}$ parameter is near to 5 cm for the considered EMEH device, for both vibration levels.

The $x_{\max}$ vs R_{load} characteristics shows that dependence on the R_{load} parameter is similar to the characteristics of the so-called matched condition in DC circuits. It is because of the relatively steady RMS value of the ε_B for each given $x_{\max}$ value.

The use of the spring bumpers significantly expands the operational frequency bandwidth – especially near the optimal val-

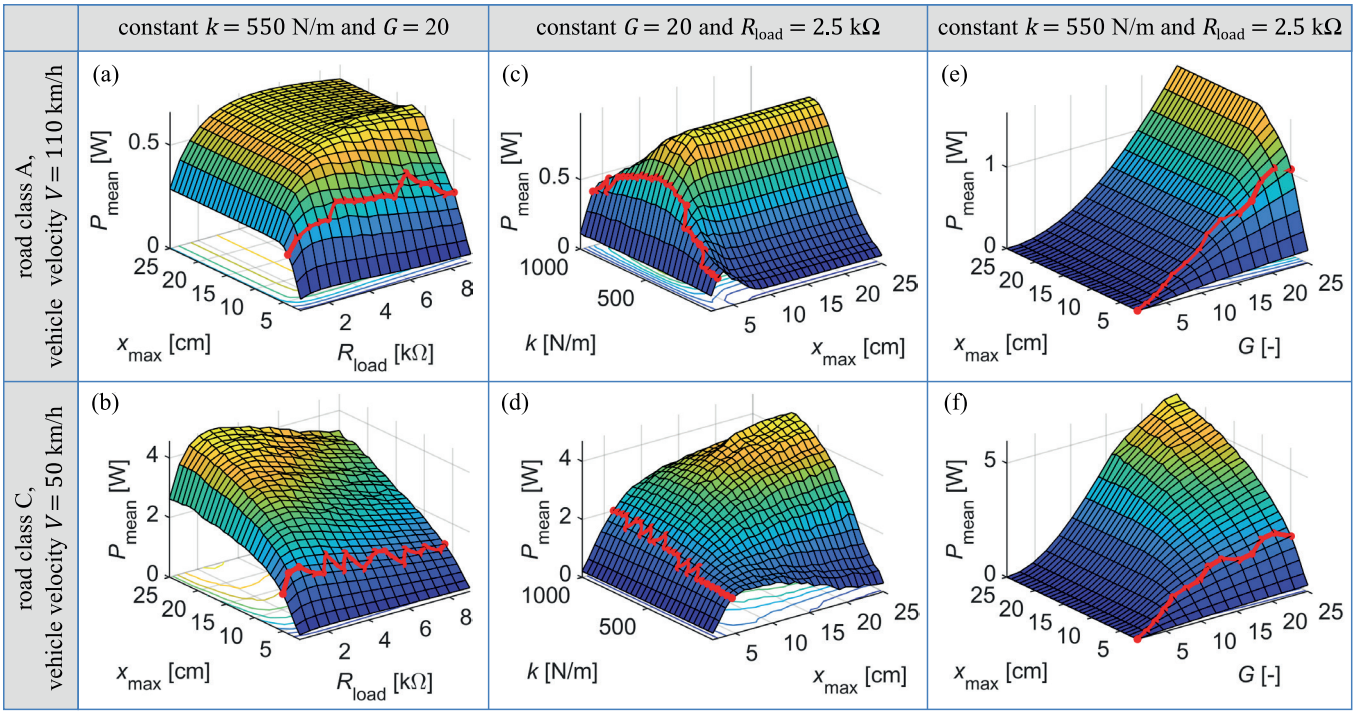

Fig. 10. Average power in dependence on respective parameters; red line denotes the best P_{mean}/x_{max} ratio

ues of the P_{mean}/x_{max} ratio marked by the red line. Thus, the characteristics falls very gently along the red line in Fig. 10(c) and (d). Due to use of the spring bumpers the system does not require the resonance effect for efficient operation. This observation stays in good agreement with the research about non-resonant impact or collision-based energy harvesters discussed in Section 1.

It can be shown that generated power is proportional to square of amplitude of excitation for linear model of the energy harvester. Thus, similarly for x_{max} values greater than amplitude of motion of the moving magnet in Fig. 10(e) the mean power seems to be proportional to the square of the gain G. When x_{max} is sufficiently small to provide collisions of the moving magnet with the spring bumpers, the square-like dependence becomes disturbed by additional nonlinearity provided by these collisions.

4.3. Nonlinearities present in the electromagnetic circuit. The question arises about the influence of the nonlinearities in Eq. (11) on the EMEH behaviour. The most important nonlinearity is collision of the moving magnet with the spring bumpers. Its influence was discussed in Subsections 4.1 and 4.2.

In this subsection the problem of nonlinearities resulting from interaction of the moving magnet with the magnetic coil is considered. Below, the nonlinear terms from Eq. (11) are listed:

- $F_{el} = \dfrac{\partial \Phi(x)}{\partial x}\dot{q} \approx \alpha(x)\dot{q}$ – electrodynamic force [N],
- $F_{rel} = \dfrac{1}{2}\dfrac{\partial L(x)}{\partial x}\dot{q}^2$ – reluctance force [N],
- $\varepsilon_L = L(x)\ddot{q} + \dfrac{\partial L(x)}{\partial x}\dot{x}\dot{q}$ – total derivative of magnetic flux linkage induced by the current in the coil over the time [V],
- $\varepsilon_B = -\dfrac{\partial \Phi(x)}{\partial x}\dot{x} \approx -\alpha(x)\dot{x}$ – electromotive force caused by the moving magnet [V].

To show the influence of changes of inductance $L(x)$ caused by the moving magnet, the values of ε_L are compared with self-induction of an air-core coil replacement ε_{Lair}. ε_{Lair} represents the self-induction which would appear for the actual state of the EMEH device for the coil inductance with neglected influence of the moving iron core (moving magnet).

The influence of the nonlinear terms listed above was analysed by the calculation of their participation in the time series describing EMEH behaviour. The equation of motion (11) was used with harmonic excitation $x_t(t) = A_t \sin \Omega t$ (without employing the quarter car model), thus $\ddot{x}_t(t) = -A_t \Omega^2 \sin \Omega t$. In this test the parameters have the following values: EMEH spring stiffness $k = 550$ N/m, load resistance $R_{load} = 2500$ Ω, $\Omega = \sqrt{k/m} = 78.1736$ rad/s, moving magnet is not limited by spring bumpers and parameter G is not used. Calculations for amplitude $A_t = 4$ mm were performed.

Results in the form of plots similar to the phase maps are shown in Fig. 11. Values of nonlinear terms are related to points (x, v) determined by the steady-state vibration of the magnet, where $v = \dot{x}$.

Numerical results in Fig. 11(a) show that the difference between ε_L and self-induction of an air-core coil replacement ε_{Lair} is significant, compared to the load voltage u_{load} of the harvester in the Fig. 11(b). Trajectories of ε_{Lair} and ε_L are strongly disturbed because of the dynamics of electrical circuit.

Figure 11(a) shows that total self-induced magnetic flux linkage change ε_L has significant values when the moving magnet is inside the coil as well as when it is near to the border of the

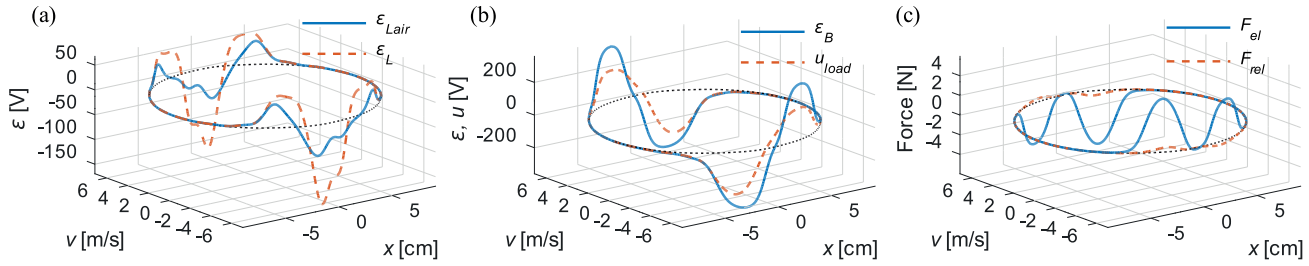

Fig. 11. Values of nonlinear terms of equation of motion for each state of the magnet in steady-state vibration for $A_t = 4$ mm and $R_{load} = 2500$: (a) self-induction of the coil ε_L compared with self-induction ε_{Lair} of air-core coil replacement, (b) electromotive force ε_B compared with voltage across the load u_{load}, (c) electrodynamic force F_{el} compared with reluctance force F_{rel}

electromagnetic coil. It follows that both greater values of the coil inductance with when the magnet is inside as well as its gradient significantly affect the EMEH device behaviour.

In this case voltage u_{load} takes smaller values than ε_B because of the losses in the coil resistance R_c and high participation of voltages induced by the current ε_L in the coil shown in Fig. 11(a). Delay and small disturbance of u_{load} are also noticeable.

The electrodynamic force F_{el} achieves opposite values to the current moving magnet velocity $v(t)$. Thus F_{el} can be interpreted as the braking force, also called electrical damping. In this case participation of the reluctance force F_{rel} is negligible.

All analysed nonlinearities have significant values. Additionally, for large amplitudes of motion the magnet does not interact with the coil in greater part of the vibration period. Hence, above some threshold value of A_t amplitude A_x grows very fast (see: Fig. 12(a)), because of smaller effective value of the electrical damping. In Fig. 12(b) wee can see that for nonlinear systems the biggest amplitude not always means the highest generated power, as it was discussed in section 1. Because for large amplitudes of motion the moving magnet interact significantly with the coil in relatively short interval we can consider

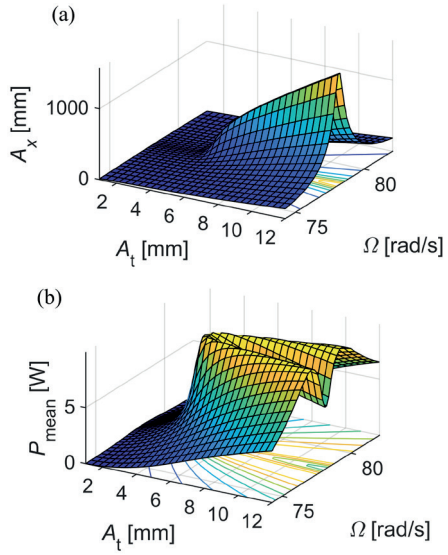

Fig. 12. (a) amplitude of the relative magnet displacement A_x and (b) mean power P_{mean} in dependence on excitation frequency and amplitude

this part of motion like near-constant velocity. In this situation amplitude of motion of the moving magnet is not important – rather the speed of the magnet crossing the coil plays important role. U-shaped curve relates to the near-optimal velocity of the magnet during crossing the coil. Lower velocity cause lower induced electromotive force ε_B however higher velocity cause that disturbances and delays shown in Fig. 11 dominate the time history of voltage and current in the EMEH electrical circuit. Then the generated power is also smaller. The u-shaped curve is not constant. Its height is proportional to the frequency, because the more frequently magnet crosses the coil the higher is the mean power P_{mean}.

From considerations above it follows that for large levels of source vibration it is profitable to apply several coils on the EMEH tube in order to extend the range of interaction of the moving magnet with the electrical circuit.

5. Conclusions

The influence of the nonlinearities of the EMEH device equipped with the mechanical amplifier and spring bumpers on the energy harvesting process has been analysed. Numerical investigation has been performed using the mathematical model of EMEH derived with aid of the Hamilton's principle of the least action. This model takes into account the dependence of the electromagnetic coil inductance on the moving magnet position. Additionally, parametric study of the influence of the different design parameters of the EMEH device on the recovered energy has been performed. Quarter car model moving on randomly generated road profiles has been employed to simulate common work conditions for the energy scavenging device.

Numerical analysis has shown that use of the mechanical amplifier together with the spring bumpers increase level of the produced energy significantly. Additionally, the spring bumpers limit the stroke of the moving magnet resulting in relatively small dimensions of the EMEH device. Moreover, it has been shown that use of spring bumpers expands operating frequency bandwidth of the EMEH device. It is valuable property for many engineering applications, in which excitation parameters are varying in time.

It has been shown that the nonlinearities included in the proposed mathematical model have a strong influence on the time histories describing dynamic behaviour of EMEH.

The proposed EMEH with its enhancements offers additional independent power supply in a vehicle and can be critical for reliable operation of its safety and navigation systems. It could be mounted on the vehicle without significant interference to structure of the lorry. The above aspects make that the proposed energy scavenging system can find a broad range of applications in automotive industry.

Acknowledgements. The research has been financed with the participation of the Smart Growth Operational Programme as a part of the project "**Innovative security and logistics management system in transportation of goods using geoinformation technologies**" [contract no. POIR.01.01.01-00-0371/17-00], financed by the European Regional Development Fund, managed by the National Centre for Research and Development in Warsaw, Poland.

REFERENCES

[1] Y. Bai, H. Jantunen, and J. Juuti, "Energy harvesting research: The road from single source to multisource", *Adv. Mater.* 30(34), 1707271 (2018), doi: 10.1002/adma.201707271.

[2] A. Tomaszuk and A. Krupa, "High efficiency high step-up dc/dc converters – a review", *Bull. Pol. Ac.: Tech.* 59(4), 475–483 (2011), doi: 10.2478/v10175-011-0059-1.

[3] W. Janke, M. Baczek, and J. Krasniewski, "Large-signal averaged models of the non-ideal flyback converter derived by the separation of variables", *Bull. Pol. Ac.: Tech.* 68(1), 81–88 (2020), doi: 10.24425/bpasts.2020.131838.

[4] C. Wei and X. Jing, "A comprehensive review on vibration energy harvesting: Modelling andrealization", *Renew. Sust. Energ. Rev.* 74, 1–18 (2017), doi: 10.1016/j.rser.2017.01.073.

[5] W. Wang, J. Cao, N. Zhang, J. Lin, and W.-H. Liao, "Magnetic-spring based energy harvesting from human motions: Design, modeling and experiments", *Energy Conv. Manag.* 132, 189–197 (2017), doi: 10.1016/j.enconman.2016.11.026.

[6] Spreemann D, Manoli Y. Electromagnetic Vibration Energy Harvesting Devices. Dordrecht: Springer; 2012, doi: 10.1007/978-94-007-2944-5.

[7] S. Yang, S.-Y. Jung, K. Kim, P. Liu, S. Lee, J. Kim, and H. Sohn, "Development of a tunable low-frequency vibration energy harvester and its application to a self-contained wireless fatigue crack detection sensor", *Struct. Health Monit.* 18(3), 920–933 (2019), doi: 10.1177/1475921718786886.

[8] J. Snamina and B. Sapinski, "Energy balance in self-powered mr damper-based vibration reduction system", *Bull. Pol. Ac.: Tech.* 59(1), 75–80 (2011), doi: 10.2478/v10175-011-0011-4.

[9] S. Lenci, "On the production of energy from sea waves by a rotating pendulum: A preliminary experimental study", *J. Appl. Nonlinear Dyn.* 3(2), 173–186 (2014), doi: 10.5890/JAND.2014.06.008.

[10] I. Shahosseini and K. Najafi, "Mechanical amplifier for translational kinetic energy harvesters", *J. Phys. Conf. Ser.* 557, 012135 (2014), doi: 10.1088/1742-6596/557/1/012135.

[11] B. Maamer, A. Boughamoura, A.M. Fath El-Bab, L.A. Francis, and F. Tounsi, "A review on design improvement sand techniques for mechanical energy harvesting using piezoelectric and electromagnetic schemes", *Energy Conv. Manag.* 199, p. 111973, 2019, doi: 10.1016/j.enconman.2019.111973.

[12] M.A. Halim, H. Cho, and J.Y. Park, "Design and experiment of a human-limb driven, frequency up-converted electromagnetic energy harvester", *Energy Conv. Manag.* 106, 393–404 (2015), doi: 10.1016/j.enconman.2015.09.065.

[13] F. Cottone, R. Frizzell, S. Goyal, G. Kelly, and J. Punch, "Enhanced vibrational energy harvester based on velocity amplification", *J. Intell. Mater. Syst. Struct.* 25(4), 443–451 (2014), doi: 10.1177/1045389X13498316.

[14] R. Frizzell, G. Kelly, F. Cottone, E. Boco, V. Nico, D. O'Donoghue, and J. Punch, "Experimental characterisation of dual-mass vibration energy harvesters employing velocity amplification", *J. Intell. Mater. Syst. Struct.* 27(20), 2810–2826 (2016), doi: 10.1177/1045389X16642030.

[15] A. Haroun, I. Yamada, and S. Warisawa, "Micro electromagnetic vibration energy harvester based on free/impact motion for low frequency – large amplitude operation", *Sens. Actuator A-Phys.* 224, 87–98 (2015), doi: 10.1016/j.sna.2015.01.025.

[16] K. Pancharoen, D. Zhu, and S.P. Beeby, "Design optimization of a magnetically levitated electromagnetic vibration energy harvester for body motion", *J. Phys. Conf. Ser.* 773, 012056 (2016), doi: 10.1088/1742-6596/773/1/012056.

[17] B. Mann and B. Owens, "Investigations of a nonlinear energy harvester with a bistable potential well", *J. Sound Vibr.* 329(9), 1215–1226 (2010), doi: 10.1016/j.jsv.2009.11.034.

[18] H. Zhang, L.R. Corr, and T. Ma, "Issues in vibration energy harvesting", *J. Sound Vibr.* 421, 79–90 (2018), doi: 0.1016/j.jsv.2018.01.057.

[19] P. Alevras and S. Theodossiades, "Vibration energy harvester for variable speed rotor applications using passively self-tuned beams", *J. Sound Vibr.* 444, 176–196 (2019), doi: 10.1016/j.jsv.2018.11.007.

[20] X. Wang, S. John, S. Watkins, X. Yu, H. Xiao, X. Liang, and H. Wei, "Similarity and duality of electromagnetic and piezoelectric vibration energy harvesters", *Mech. Syst. Signal Proc.* 52-53, 672–684 (2015), doi: 10.1016/j.ymssp.2014.07.007.

[21] K. Kecik, A. Mitura, S. Lenci, and J. Warminski, "Energy harvesting from a magnetic levitation system", *Int. J. Non-Linear Mech.* 94, 200–206 (2017), doi: 10.1016/j.ijnonlinmec.2017.03.021.

[22] N.G. Elvin and A.A. Elvin, "An experimentally validated electromagnetic energy harvester", *J. Sound Vibr.* 330(10), 2314–2324 (2011), doi: 10.1016/j.jsv.2010.11.024.

[23] T. Sobczyk and M. Radzik, "Improved algorithm for periodic steady-state analysis in nonlinear electromagnetic devices", *Bull. Pol.Ac.: Tech.* 67(5), 863–869 (2019), doi: 10.24425/bpasts.2019.130878.

[24] T. Lubin, K. Berger, and A. Rezzoug, "Inductance and force calculation for axisymmetric coil systems including an iron core of finite length", *Prog. Electromagn. Res. B* 41, 377–396 (2012), doi: 0.2528/PIERB12051105.

[25] A. Preumont, *Mechatronics – Dynamics of Electromechanical and Piezoelectric Systems*, Netherlands: Springer, 2006, doi: 10.1007/1-4020-4696-0.

[26] I. Zaabar and K. Chatti, "Identification of localized roughness features and their impact on vehicle durability", in *11th International Symposium on Heavy Vehicle Transportation Technology*, 2010.

[27] T.F. Tyan, Y.-F. Hong, R. Shun, H. Tu, and W. Jeng, "Generation of random road profiles", *J. Adv. Eng.* 4, 151–156 (2009).